New Phytologist

Research

Stomatal optimization based on xylem hydraulics (SOX) improves land surface model simulation of vegetation responses to climate

Cleiton B. Eller[1,2], Lucy Rowland[1], Maurizio Mencuccini[3,4], Teresa Rosas[3,4], Karina Williams[5], Anna Harper[6], Belinda E. Medlyn[7], Yael Wagner[8], Tamir Klein[8], Grazielle S. Teodoro[9], Rafael S. Oliveira[2], Ilaine S. Matos[10], Bruno H. P. Rosado[10], Kathrin Fuchs[11], Georg Wohlfahrt[12], Leonardo Montagnani[13], Patrick Meir[14,15], Stephen Sitch[1] and Peter M. Cox[6]

[1]College of Life and Environmental Sciences, University of Exeter, Exeter, EX4 4QF, UK; [2]Department of Plant Biology, University of Campinas, Campinas 13083-862, Brazil; [3]CREAF, Bellaterra 08193, Barcelona, Spain; [4]ICREA, Pg. Lluís Companys 23 08010, Barcelona, Spain; [5]Met Office Hadley Centre, Fitzroy Road, Exeter, EX1 3PB, UK; [6]College of Engineering, Mathematics and Physical Sciences, University of Exeter, Exeter, EX4 4QF, UK; [7]Hawkesbury Institute for the Environment, Western Sydney University, Locked Bag 1797, Penrith, NSW 2751,Australia; [8]Department of Plant & Environmental Sciences, Weizmann Institute of Science, 76100, Rehovot, Israel; [9]Institute of Biological Sciences, Federal University of Pará, Belém 66075-110, Brazil; [10]Department of Ecology – IBRAG, Rio de Janeiro State University (UERJ), Rio de Janeiro 20550-013, Brazil; [11]Department of Environmental Systems Science, ETH Zurich, Universitätstrasse 2 8092, Zurich, Switzerland; [12]Department of Ecology, University of Innsbruck, Innsbruck 6020, Austria; [13]Forest Services, Autonomous Province of Bolzano, Via Brennero 6 39100, Bolzano, Italy; [14]Research School of Biology, The Australian National University, Acton, ACT 2601, Australia; [15]School of Geosciences, University of Edinburgh, Edinburgh, EH9 3FF,UK

Author for correspondence:
Cleiton B. Eller
Tel: +44 07864 755668
Email: c.breder-eller@exeter.ac.uk

Received: *5 November 2019*
Accepted: *3 January 2020*

New Phytologist (2020)
doi: 10.1111/nph.16419

Key words: climate change, drought, eddy covariance, land-surface models, stomatal optimization, xylem hydraulics.

Summary

- Land surface models (LSMs) typically use empirical functions to represent vegetation responses to soil drought. These functions largely neglect recent advances in plant ecophysiology that link xylem hydraulic functioning with stomatal responses to climate.
- We developed an analytical stomatal optimization model based on xylem hydraulics (SOX) to predict plant responses to drought. Coupling SOX to the Joint UK Land Environment Simulator (JULES) LSM, we conducted a global evaluation of SOX against leaf- and ecosystem-level observations.
- SOX simulates leaf stomatal conductance responses to climate for woody plants more accurately and parsimoniously than the existing JULES stomatal conductance model. An ecosystem-level evaluation at 70 eddy flux sites shows that SOX decreases the sensitivity of gross primary productivity (GPP) to soil moisture, which improves the model agreement with observations and increases the predicted annual GPP by 30% in relation to JULES. SOX decreases JULES root-mean-square error in GPP by up to 45% in evergreen tropical forests, and can simulate realistic patterns of canopy water potential and soil water dynamics at the studied sites.
- SOX provides a parsimonious way to incorporate recent advances in plant hydraulics and optimality theory into LSMs, and an alternative to empirical stress factors.

Introduction

Large areas of the globe will be exposed to increased aridity in the near future (Sheffield & Wood, 2008; Duffy *et al.*, 2015; Marengo *et al.*, 2018). As drought events become more intense and frequent, accurately representing vegetation–climate feedbacks in Earth system models (ESMs) is increasingly important, as these interactions can drastically influence model projections of global climate change (Cox *et al.*, 2000). The current generation of land surface models (LSMs) does not accurately simulate vegetation carbon dynamics during drought (Sitch *et al.*, 2008; Powell *et al.*, 2013; Medlyn *et al.*, 2016; Ukkola *et al.*, 2016; Restrepo-Coupe *et al.*, 2017; Rogers *et al.*, 2017; Eller *et al.*, 2018b), thereby restricting our capability to predict the effect of increased aridity on vegetation distribution and its feedbacks on the global carbon cycle and climate. Many LSMs represent the effects of reduced soil moisture on canopy carbon assimilation (A) using an empirical drought factor commonly referred as β-factor (Cox *et al.*, 1998). The β-factor approach has been shown to overestimate plant responses to seasonal and experimentally induced drought (Ukkola *et al.*, 2016; Restrepo-Coupe *et al.*, 2017; Eller *et al.*, 2018b). The β-factor has a large impact on the modelled global carbon budget, supressing 30–40% of the annual gross primary productivity (GPP) in large areas of arid and semiarid ecosystems (Trugman *et al.*, 2018). Despite its importance, there is scarce empirical support for the drought

functions used in most LSMs (Medlyn *et al.*, 2016). The lack of a theoretical or empirical basis for the β-factor implies an urgent need for new modelling approaches to replace this important component of LSMs so as to improve our capacity to predict vegetation–climate interactions.

Stomatal responses of plants to soil drought involve complex chemical signalling and hydrodynamic processes in leaf cells, some of which have not been entirely elucidated (Buckley, 2017, 2019; Qu *et al.*, 2019). Stomatal optimization models are a useful approach to model stomatal behaviour that circumvents the need to explicitly represent the physiological processes involved in stomatal regulation. Optimization models employ a 'goal-oriented' approach, assuming that plant stomata behaviour has been selected through plant evolutionary history to maximize a given objective function (Cowan, 2002; Dewar *et al.*, 2009; Prentice *et al.*, 2014; Buckley, 2017). The traditional approach to model optimal stomatal behaviour is derived from the seminal work of Cowan & Farquhar (1977). This approach proposes that optimal stomatal behaviour maximizes A minus the carbon cost of water lost (λE) over a given time interval, where E is transpiration and λ is the Lagrange multiplier that represents the carbon cost of a unit of water lost. This model, hereafter labelled CF, after Cowan and Farquhar, is capable of simulating many patterns of stomatal responses to climate over short timescales (Farquhar *et al.*, 1980; Berninger & Hari, 1993), and has provided the theoretical basis for several widely used semi-empirical stomatal models (Jacobs, 1994; Leuning, 1995; Medlyn *et al.*, 2011). However, CF predicts that stomatal conductance (g_s) increases in response to elevated CO_2 when A is Rubisco-limited, which contradicts most observations (Mott, 1988; Medlyn *et al.*, 2001). Other limitations are related to the λ, as the CF hypothesis does not link λ to measurable plant traits or environmental quantities (Buckley, 2017), and assumes λ is constant over the period of reference (Cowan & Farquhar, 1977), which makes the original CF unable to predict long-term g_s decline in response to soil moisture depletion.

Since the original CF work, many attempts have been made to incorporate the effects of declining soil moisture in the CF stomatal optimization framework (Cowan, 1986; Mäkelä *et al.*, 1996; Williams *et al.*, 1996; Manzoni *et al.*, 2013). Some of these attempts, such as the soil–plant–atmosphere (SPA) model of Williams *et al.* (1996), employ principles of plant hydraulics to constrain stomatal optimization and have been successfully incorporated into LSMs (Bonan *et al.*, 2014). The numerical approach used by SPA employs a hydraulic threshold to set a lower water potential limit (Ψ_{min}) for g_s, which simulates a strict isohydric stomatal regulation (Fisher *et al.*, 2006). Despite using plant hydraulics, SPA still relies on a water-use efficiency optimization similar to CF to model stomatal behaviour when $\Psi > \Psi_{min}$ (Williams *et al.*, 1996; Bonan *et al.*, 2014).

Alternative routes to model plant optimal stomatal behaviour have been proposed recently (for a review, see Mencuccini *et al.*, 2019a). These approaches circumvent the CF limitations by assuming that plant optimal stomatal behaviour minimizes the instantaneous fitness costs associated with low Ψ. These new optimization models use widely available plant hydraulic traits (Kattge *et al.*, 2011; Choat *et al.*, 2012) to simulate g_s responses to environmental conditions, producing a realistic g_s decline in response to elevated atmospheric CO_2 and soil drought (Sperry *et al.*, 2017; Venturas *et al.*, 2018; Eller *et al.*, 2018b; Wang *et al.*, 2019). This approach predicts a tight coordination between stomatal and xylem functioning which is widely corroborated by observations (Hubbard *et al.*, 2001; Meinzer *et al.*, 2009; Klein, 2014). Another advantage of this approach is its capacity to simulate a diversity of contrasting stomatal behaviours, from iso- to anisohydric (Martinez-Vilalta *et al.*, 2014; Klein, 2014).

Sperry *et al.* (2017) proposes a model that assumes that, as xylem hydraulic conductance declines, the increased risk of hydraulic failure is the main fitness cost associated with low Ψ. Eller *et al.* (2018b) adapted the Sperry *et al.* (2017) model into the stomatal optimization model based on xylem hydraulics (SOX), which differs from the Sperry *et al.* (2017) model principally by using a different optimization target. The SOX optimization target is based on the PGEN model (Friend, 1995), which assumes that stomata optimize plant dry matter production, represented by the product of photosynthesis and a linear function of Ψ. The SOX model in Eller *et al.* (2018b) uses a numerical routine to find the optimum g_s. However, the PGEN optimization target can also be found analytically (Friend & Cox, 1995; Dewar *et al.*, 2018). A parsimonious analytical formulation for SOX would facilitate its incorporation into existing LSMs and provide a practical alternative to the β-function for modelling stomatal responses to drought at global scales.

In this study we develop an analytical approximation for the numerical SOX model presented in Eller *et al.* (2018b). We then create a new configuration for the Joint UK Land Environment Simulator (JULES; Best *et al.*, 2011; Clark *et al.*, 2011) that uses SOX to compute vegetation g_s from environmental and plant hydraulic data. Using a global dataset of xylem hydraulic traits, together with an extensive leaf gas-exchange and eddy covariance dataset, we calibrate the SOX parameters and compare the JULES-SOX performance to the default JULES using the β-function, across all major global biomes. Our goals in this paper are twofold: to test SOX agreement with global observations of g_s to assess the generality of the underlying hypothesis in SOX, that is, that plant stomata evolved to balance carbon assimilation with the loss of hydraulic conductance; and to evaluate the effect of SOX on JULES ecosystem-scale predictions of carbon and water fluxes, and their agreement with observations.

Materials and Methods

Analytical SOX description

The SOX central hypothesis can be summarized as 'stomatal conductance (g_s) is such as to maximize the product of leaf photosynthesis and xylem hydraulic conductance' and is given by:

$$A[c_i(g_s)]K[\Psi_m(g_s)], \qquad \text{Eqn 1}$$

where A is leaf net CO_2 assimilation (mol CO_2 m^{-2} s^{-1}), which is a function of leaf internal CO_2 partial pressure (c_i, in Pa),

which is itself a function of stomatal conductance to CO_2 (g_s, mol m^{-2} s^{-1}). The K is the normalized (0–1) xylem hydraulic conductance computed as:

$$K(\Psi) = \frac{1}{[1 + (\Psi/\Psi_{50})^a]}, \quad \text{Eqn 2}$$

where Ψ_{50} is Ψ when $K = 0.5$ and the parameter a gives the shape of the curve, with a higher a producing a steeper response to Ψ. We use the mean (Ψ_m, MPa) of the canopy water potential at the predawn (Ψ_{pd}, MPa) and the canopy water potential (Ψ_c, MPa) to compute K with Eqn 2 to account for the gradual decline in Ψ along the soil to canopy hydraulic pathway (see details in Supporting Information Notes S1). The g_s value that maximizes Eqn 1 is found at:

$$\frac{\partial AK}{\partial g_s} = 0. \quad \text{Eqn 3}$$

The g_s value that satisfies Eqn 3 was found numerically in Eller *et al.* (2018b), but a computationally efficient analytical solution is preferable for application in dynamic global vegetation models (DGVMs) and ESMs. We developed an analytical approximation for the optimal SOX g_s using the partial derivatives of A with respect to c_i and K with respect to Ψ_m. All steps of the model derivation are described in Notes S1. The resulting SOX equation for the optimal g_s is:

$$g_s = 0.5\frac{\partial A}{\partial c_i}\left(\sqrt{\frac{4\xi}{\partial A/\partial c_i} + 1} - 1\right), \quad \text{Eqn 4}$$

The benefit of stomatal opening is represented here by the sensitivity of leaf photosynthesis to the internal CO_2 concentration ($\partial A/\partial c_i$). By contrast, the parameter ξ represents the cost of stomatal opening in terms of loss of xylem conductivity under low Ψ_{pd} and/or higher leaf-to-air vapour pressure (D, mol mol^{-1}):

$$\xi = \frac{2}{1/K\partial K/\partial \Psi_m r_p 1.6D}. \quad \text{Eqn 5}$$

Low ξ indicates high hydraulic costs occurring during drought (i.e. lower Ψ_{pd} and higher D; Fig. S1). SOX simulates dynamic changes on the plant hydraulic resistance (r_p), computing r_p as a function of Ψ_{pd} and the plant minimum hydraulic resistance (r_{pmin}, m^2 s MPa mol^{-1} H_2O):

$$r_p = \frac{r_{p,min}}{K(\Psi_{pd})}. \quad \text{Eqn 6}$$

Solving SOX main equations (Eqns 4, 5) requires computing the partial derivatives of A and K, $\partial A/\partial c_i$ and $\partial K/\partial \Psi_m$, respectively. These derivatives were estimated numerically in this study as described in Notes S2.

We evaluated SOX as a stand-alone leaf-level model, and coupled to JULES (hereafter JULES-SOX). The leaf-level model was evaluated against leaf gas exchange data as an 'assumption centred' (*sensu* Medlyn *et al.*, 2015) test of the hypothesis underlying SOX. The JULES-SOX was then evaluated against ecosystem-level eddy flux data, which constituted the first practical test of the utility of SOX for LSMs.

JULES β-function description

The JULES model (Best *et al.*, 2011; Clark *et al.*, 2011) uses the Collatz *et al.* (1991, 1992) photosynthesis model for C_3 and C_4 plants (Notes S3) to produce unstressed rates of A based on the colimitation of light, Rubisco carboxylation capacity, and the transport of photoassimilates (for C_3 plants) and PEPcarboxylase limitation (for C_4 plants). The effect of soil moisture in A in the default JULES is given by multiplying A by the β factor, computed using the β-function from Cox *et al.* (1998):

$$\beta = \begin{cases} 1 & \text{for} \quad \theta > \theta_c \\ \frac{\theta - \theta_w}{\theta_c - \theta_w} & \text{for} \quad \theta_w < \theta \le \theta_c \\ 0 & \text{for} \quad \theta \le \theta_w \end{cases}, \quad \text{Eqn 7}$$

where θ is the mean soil moisture in the root zone (m^3 m^{-3}), and θ_c and θ_w, are the critical and wilting points, which are defined by Cox *et al.* (1998) as the θ when soil Ψ is -0.033 and -1.5 MPa, respectively. The default JULES formulation employs the Jacobs (1994) equation to predict c_i from D, c_a and the CO_2 compensation point, Γ (Pa):

$$c_i = f_0\left(1 - \frac{D}{D_{crit}}\right)(c_a - \Gamma), \quad \text{Eqn 8}$$

where f_0 and D_{crit} are empirical parameters (Jacobs, 1994; Cox *et al.*, 1998).

The JULES-SOX configuration replaces Eqns 7 and 8, computing g_s from environmental data and plant hydraulic inputs with Eqns 4 and 5. To compute A from the g_s predicted by Eqn 4, we solved the limiting photosynthetic rates from the Collatz *et al.* (1991, 1992) model as functions of c_a and g_s, as described in Notes S3.

Leaf-level SOX evaluation

We used a global compilation of leaf gas exchange data to evaluate the SOX capacity to reproduce leaf stomatal responses of a wide range of woody plants. This dataset contains observations compiled by Lin *et al.* (2015), complemented with other published and unpublished data (see Table S1 and Fig. S2 for additional information). In total, there are 3597 measurements of g_s and Ψ_{pd} together with environmental variables used for driving the model, that is, incident photosynthetic active radiation (I_{par}), air temperature (T_a), c_a and D. These data come from 30 woody plant species collected in 15 sites around the world (Fig. S2b). The Ψ_{pd} was measured on the same day as g_s, and the

environmental data was measured simultaneously with g_s. The dataset included field and glasshouse observations, with environmental conditions varying from well-watered to extreme drought ($\Psi_{pd} = -7$ MPa). These observations were grouped into the global plant functional type (PFT) categories from Harper *et al.* (2016) (Table 1). Harper *et al.* (2016) divides angiosperm tree species into broadleaf evergreen tropical trees (BET-Tr), broadleaf evergreen temperate trees (BET-Te) and broadleaf deciduous trees (BDT), while gymnosperms tree species are divided into needleleaf evergreen trees (NET) and needleleaf deciduous trees (NDT). Shrub species were divided into evergreen shrubs (ESh) and deciduous shrubs (DSh), and two grass PFTs defined by their photosynthetic pathway (C_3 and C_4). The grass PFTs and the NDT were excluded from the leaf-level evaluation because no stomatal conductance data were available for these PFTs in the dataset used in this study.

The plant hydraulic parameters used in SOX (i.e. Ψ_{50}, a, and r_{pmin}) were fitted to the g_s data using an algorithm that minimizes the model residual sum of squares within the constraints of the observed Ψ_{50}, a and r_{pmin}. We compiled hydraulic data for each PFT from the literature to constrain the leaf-level model fit. The Ψ_{50} for woody plants was obtained from a version of the Choat *et al.* (2012) dataset updated recently by Mencuccini *et al.* (2019b). The shape parameter a of the xylem vulnerability function (Eqn 2) was estimated from the linear gradient between Ψ_{50} and the Ψ when the plant loses 88% of its maximum hydraulic conductance. The r_{pmin} was estimated from branch-level hydraulic conductivity measurements scaled from branch to whole plant, taking into account plant height, Huber value and xylem tapering using the calculations described in Christoffersen *et al.* (2016) and Savage *et al.* (2010) (Notes S4). All the data used for these calculations were obtained from the hydraulic dataset from Mencuccini *et al.* (2019b). We note that scaling branch to whole tree r_{pmin} requires several assumptions about tree hydraulic architecture (Notes S4). Therefore, the presented values of r_{pmin} must be considered as a reference useful only to assess if the r_{pmin} input values used in the model are within the same order of magnitude of the observations. The other parameters of the photosynthesis model used in SOX (Notes S3) were set equal to those in Harper *et al.* (2016).

Table 1 Residual sum of squares (RSS), number of leaf-level stomatal conductance observations (*N*) used to fit *n* parameters to the data, and the resulting Akaike information criterion differences (ΔAIC) between stomatal optimization based on xylem hydraulics (SOX) and the β-function.

		SOX		β-function		
PFT	*N*	RSS	*n*	RSS	*n*	ΔAIC
BET-Tr	434	4.83	3	6.53	2	−126.1
BET-Te	1334	19.68	3	37.37	2	−853.2
BDT	71	3.48	3	3.04	2	11.6
NET	1571	0.65	3	2.29	2	−1926.4
ESh	133	3.37	3	7.94	2	−112
DSh	64	2.76	3	8.03	2	−66.4

PFT, plant functional type; BET-Tr, broadleaf evergreen tropical tree; BET-Te, broadleaf evergreen temperate tree; BDT, broadleaf deciduous tree; NET, needleleaf evergreen tree; ESh, evergreen shrubs; DSh, deciduous shrubs.

The model predictive skill was evaluated using the model root-mean-square errors (RMSE) and the Nash & Sutcliffe (1970) model efficiency index (NSE). The NSE varies from $-\infty$ to 1, with 1 indicating perfect agreement between model and observations, while NSE < 0 indicates that the mean value of the observations is a better predictor than the model. The model parsimony was evaluated using the Akaike information criterion (AIC), which penalizes model overparameterization (Bozdogan, 1987). We compared SOX AIC score with the β-function (Eqns 7, 8). The parameters f_0 and D_{crit}, (Eqn 8) were fitted to the PFT g_s data, while θ_c and θ_w were held at their default values (−0.033 and − 1.5 MPa, respectively).

The uncertainty in plant hydraulic parameters caused by within-PFT hydraulic variability was propagated to the model predictions using bootstrapped 95% confidence intervals. We created the interval based on 1000 model runs with parameters resampled from the hydraulic trait data for each PFT.

Eddy-covariance based JULES-SOX evaluation

We evaluated default JULES and JULES-SOX against daily GPP estimates derived from eddy flux tower data at 62 FLUXNET sites (http://fluxnet.fluxdata.org, Baldocchi *et al.*, 2001) and eight LBA sites (https://daac.ornl.gov/LBA, Saleska *et al.*, 2013), covering all the major biomes of the world (Fig. S2; Table S2). In 10 of these sites we also had data for surface (5–15 cm) soil moisture content, which was used to evaluate the model soil moisture dynamics predictions. We classified the land cover on each site using the International Geosphere-Biosphere Programme (IGBP) classification (Loveland *et al.*, 2000). Each site was classified as one of the following categories according to its prescribed PFT cover (Table S2): cropland (CRO), deciduous broadleaf forests (DBF), deciduous needleleaf forests (DNF), temperate evergreen broadleaf forests (EBF-Te), tropical evergreen broadleaf forests (EBF-Tr), evergreen needleleaf forest (ENF), grassland (GRA), mixed forest (MF), savannah (SAV), shrubland (SHR) and wetlands (WET). We grouped the IGBP categories open and closed shrublands into SHR, as we only had a single closed shrubland site. Similarly, woody savannah was grouped with SAV, as we only had two woody savannah sites. We divided the evergreen broad leaf forests category into EBF-Te and EBF-Tr, as these sites were dominated by distinct PFTs (BET-Te and BET-Tr, respectively).

We evaluated JULES-SOX using the SOX hydraulic parameters (i.e. Ψ_{50}, a, and r_{pmin}) that minimized the residual sum of squares between SOX predictions and the eddy flux GPP observations from a subset of the sites used for model evaluation (Fig. S2; Table S2). Each site was used to calibrate the hydraulic parameters for its dominant PFT (i.e. the PFT covering > 50% of the site area), except for DSh, which was not dominant in any of the available sites. We used a site with DSh cover of 35% (US-SRM) to calibrate the hydraulic parameters of this PFT. The hydraulic parameters of the others PFTs (if any) present on the site were kept constant during the model runs for parameter

calibration. Similar to the leaf-level evaluation, the parameter calibration in JULES-SOX was constrained within the range of the observed values of Ψ_{50}, a, and r_{pmin} for all PFTs, except for NDT, which did not have enough observations to satisfactorily constrain the model parameters. The Ψ_{50} for grasses was obtained from the Lens *et al.* (2016) dataset updated with data from Ocheltree *et al.* (2016).

Model setup

The JULES and JULES-SOX configurations used in this study employed the 10-layer canopy scheme with sunlit and shaded leaves in each layer as described in Clark *et al.* (2011). The canopy radiation profile was given by the two-stream approach from Sellers (1985), with the sun-fleck penetration scheme from Mercado *et al.* (2009), and an exponential decrease of photosynthetic capacity through the canopy (Mercado *et al.*, 2007). All the model runs used in this study were site-level simulations driven with hourly local meteorological data. Vegetation dynamics (Cox, 2001) was turned off and the site PFT coverage by site was prescribed based on the site vegetation description obtained from the site principal investigators (Table S2) or information from the site available on the FLUXNET website (https://fluxnet.fluxdata.org/sites/site-list-and-pages/). Site soil hydraulic properties were parameterized using Brooks & Corey (1964) relations. These properties were derived from data collected at each site or, when local data were not available, calculated from the sand/silt/clay fractions in the nearest gridbox in the high-resolution input file to the Met Office Central Ancillary Program (Dharssi *et al.*, 2009), using approximations from Cosby *et al.* (1984). The model was spun up by recycling the meteorological data at each site for up to 50 yr.

Results

SOX sensitivity to environmental and hydraulic drivers

The SOX analytical approximation (Eqns 4, 5) has g_s responses to climate which are consistent with the patterns commonly reported in the literature (Mott, 1988; Leuning, 1995; Dewar *et al.*, 2018). The g_s responses to I_{par} and c_a in SOX (Fig. 1a) are given by the $\partial A/\partial c_i$ gradient decreasing at low light because of the changes in the light response curve, as A starts being limited by light (Notes S3), or at high c_a (Notes S2). SOX correctly predicted stomatal closure in response to increased c_a under Rubisco-limited conditions (Mott, 1988; Fig. 1a). The classical exponential g_s responses to D (Leuning, 1995) was reproduced in SOX (Fig. 1a) through the D effect on ξ (Eqn 5; Fig. S1a). An exponential g_s decline was also predicted by SOX in response to decreasing Ψ_{pd} (Fig. 1a), which summarizes both the responses to the soil water availability in the root zone and the hydraulic stress of transporting water to the top of the canopy (Eqn S1.2 in Notes S1). The plant hydraulic parameters modulated the model sensitivity to D or Ψ_{pd} (Fig. 1b–d), with a less negative Ψ_{50} or a higher r_{pmin} increasing the g_s sensitivity to Ψ_{pd} and D (Fig. 1c,d). The effect of the vulnerability curve shape parameter a was more complex: lower a increased g_s sensitivity to less negative Ψ_{pd}, but decreased g_s sensitivity to very negative Ψ_{pd} values (Fig. 1c).

The patterns produced by the analytical SOX were similar to the numerical version from Eller *et al.* (2018b), with a correlation coefficient ranging from 0.92 to 1 (Fig. S3). However, the use of linear gradients in Eqns 4 and 5 (Notes S2) can cause discrepancies between the different model versions under certain ranges of environmental conditions. The analytical version of SOX underestimated g_s at low D (Fig. S3), overestimated g_s at low c_a, and g_s increased faster in response to light (Fig. S3) than in the numerical model.

SOX leaf-level evaluation

Stomatal optimization based on xylem hydraulics simulated the observed leaf-level g_s responses to soil drought better than the β-function in all the studied woody PFTs, except BDT (Fig. 2). The β-function predicted that all PFTs will reach $g_s = 0$ at $\Psi_{pd} > -2$ MPa, whereas SOX predicted $g_s > 0$ even when $\Psi_{pd} < -4$ MPa in some PFTs (Fig. 2b,e). The less conservative stomatal behaviour predicted by SOX produced a NSE that was, on average, 0.65 higher and a RMSE that was 26% lower than the β-function. Most of the observed g_s was within SOX 95% confidence bounds derived from the hydraulic parameters' uncertainty (shaded region in Fig. 2). The only values outside SOX uncertainty boundaries were the highest g_s values in BET-Tr and BET-Te (Fig. 2a,b), and the lowest NET g_s values when $\Psi_{pd} > -3.5$ MPa (Fig. 2d).

Stomatal optimization based on xylem hydraulics produced a better fit to the g_s data, which resulted in a lower AIC than the β-function for all PFTs, except BDT (Table 1). Fitting the two empirical parameters of the Jacobs (1994) equation (f_0 and D_{crit}; Eqn 8) to the g_s data results in a β-function AIC score that is 512.1 higher than SOX (Table 1). For the BDT observations, the β-function results in an AIC score that is 11.6 lower than SOX. Our BDT observations were restricted to relatively well-watered conditions (lowest Ψ_{pd} was − 1.2 MPa), which limits the utility of this dataset to evaluate the model responses to soil drought.

JULES-SOX site-level calibration

The hydraulic parameters that maximized the JULES-SOX fit to the GPP data at the calibration sites (Table S2; Fig. S2) were within 1 SD of the mean observed hydraulic parameters for most PFTs (Table 2). The gymnosperm PFTs (NDT and NET) required Ψ_{50} values 1.6 MPa less negative than their observed Ψ_{50} means to fit the GPP data, which is lower than the observed SD range but still within the range of Ψ_{50} observations for NET (Ψ_{50} ranges from − 2.3 to − 7.5 MPa in NET). The NDT and BET-Tr calibrated a were also slightly lower than the SD range (Table 2), but within the observed a range for BET-Tr (a ranges from 1.8 to 7.8 in BET-Tr). The only PFT with a calibrated r_{pmin} outside the SD range of the mean r_{pmin} was ESh (Table 2).

The monthly GPP modelled by JULES-SOX fitted the eddy covariance GPP data better than the default JULES in eight out

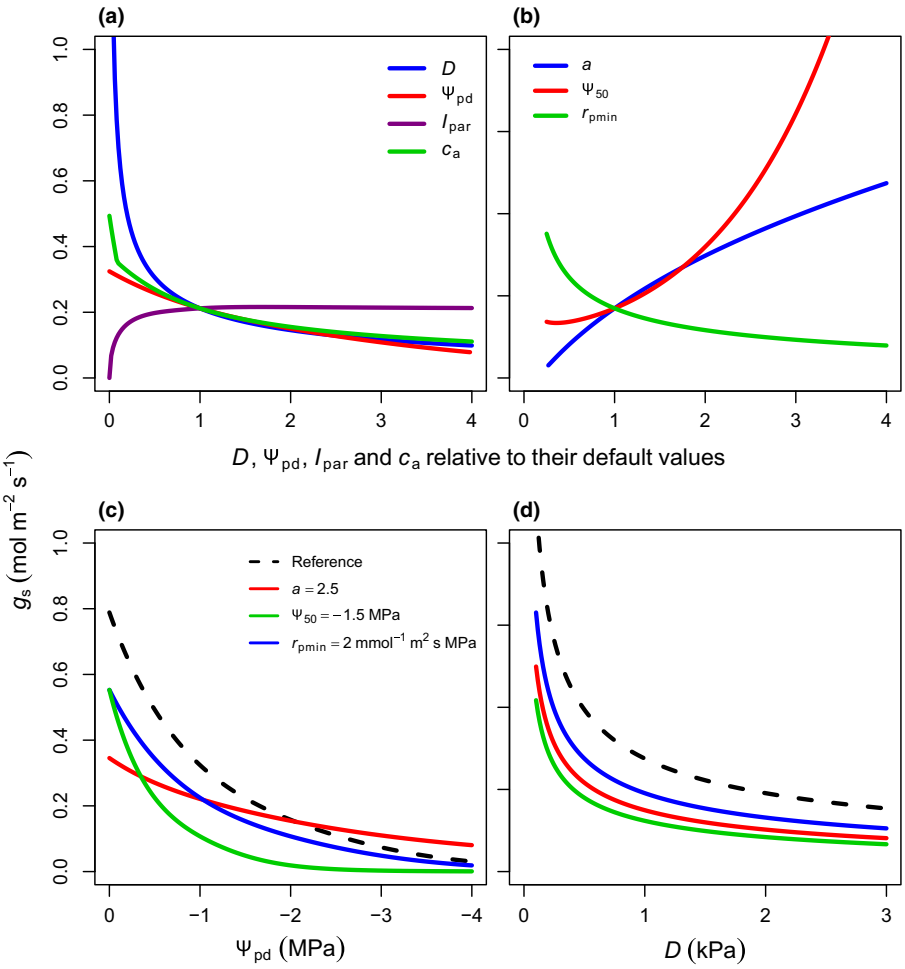

Fig. 1 (a, b) Stomatal conductance (g_s) sensitivity to environmental drivers (a) and plant hydraulic traits (b) as modelled by stomatal optimization based on xylem hydraulics (SOX) (D, vapour pressure deficit; Ψ_{pd}, predawn water potential; I_{par}, incident photosynthetically active radiation; c_a, atmospheric CO_2 partial pressure; Ψ_{50}, Ψ when plant loses 50% of its maximum conductance; a, shape of vulnerability function; r_{pmin}, minimum plant hydraulic resistance). Variables were changed individually while the others were held constant at their reference values (D = 0.5 kPa, Ψ_{pd} = −0.5 MPa, I_{par} = 600 μmol m^{-2} s^{-1}, c_a = 36 Pa, Ψ_{50} = −2 MPa, a = 3, r_{pmin} = 1 m^2 s MPa $mmol^{-1}$). For (c) and (d) the reference lines (dashed black) represent values of Ψ_{50} = −3 MPa, a = 5, r_{pmin} = 1 $mmol^{-1}$ m^2 s MPa, and the coloured lines show how changing each hydraulic parameter affects g_s response to Ψ_{pd} and D. In (c) and (d), I_{par} was set to 2000 μmol m^{-2} s^{-1}. The Rubisco maximum carboxylation rate at 25°C (V_{cmax25}) was set to 100 μmol m^{-2} s and the rest of the photosynthetic parameters follow the broadleaf evergreen tropical tree (BET-Tr) parameterization from Harper *et al.* (2016).

of the nine sites used for parameter calibration (Table S2; Figs 3, S2). The default JULES NSE was 0.01 higher in the DSh site (Fig. 3i), whereas in all the other sites JULES-SOX had a better fit. The difference between JULES-SOX and default JULES NSE ranged from 0.03 for C3 grasses (Fig. 3f) to 11.44 for BET-Tr (Fig. 3a). The large improvement in the BET-Tr site was caused by the lower GPP decline predicted by SOX during January–March and September–December. The decline in BET-Tr GPP in default JULES can be attributed to the β-factor overestimating the effects of soil moisture on the vegetation carbon assimilation during drier periods (Fig. S4a). On average, JULES-SOX NSE for GPP was 1.59 higher than default JULES, while its RMSE was 38% lower than JULES.

The less conservative stomatal behaviour predicted by SOX resulted in higher evapotranspiration rates throughout the year (Figs S5, S6), which depleted soil moisture to lower values than the β-function in default JULES during drier periods (Figs S4, S7). The soil moisture dynamics from JULES-SOX are more closely aligned with the monthly soil moisture observations in eight out of the 10 sites where soil moisture data were available (Fig. S7). JULES-SOX NSE for monthly soil moisture was 1.67 higher and RMSE was 19% lower than default JULES. JULES-SOX also simulates realistic Ψ_c for most PFTs (Figs 4, S4). The modelled Ψ_c at the calibration sites is within the interquartile range of the observed minimum Ψ_c at midday for all woody PFTs, except NDT (Fig. 4).

Biome-level JULES-SOX evaluation

Using JULES-SOX with calibrated SOX hydraulic parameters produced a better fit to the GPP data than default JULES for 50 out of the 70 eddy flux evaluation sites (Tables 3, S2; Fig. 5). Across all biomes the JULES-SOX median NSE was 0.19 higher than default JULES, and its RMSE was 19% lower (Table 3). The difference between JULES-SOX and JULES skill was highest at EBF-Tr sites, which have a median NSE 3.18 higher and RMSE 45% lower in JULES-SOX (Table 3; Fig 5a). The fit of EBT-Te to data was also improved substantially by JULES-SOX, with JULES-SOX having a median NSE 1.01 higher and RMSE 18% lower (Fig. 5a; Table 3). Default JULES only outperformed JULES-SOX at CRO, which had a median NSE 0.08 lower in JULES-SOX, and GRA, where the RMSE 5% was higher in JULES-SOX (Fig. 5a; Table 3).

Default JULES significantly underestimated the observed mean annual GPP by 143.3 g C m^{-2} across all biomes, which corresponds to 13.6% of the observed mean annual GPP

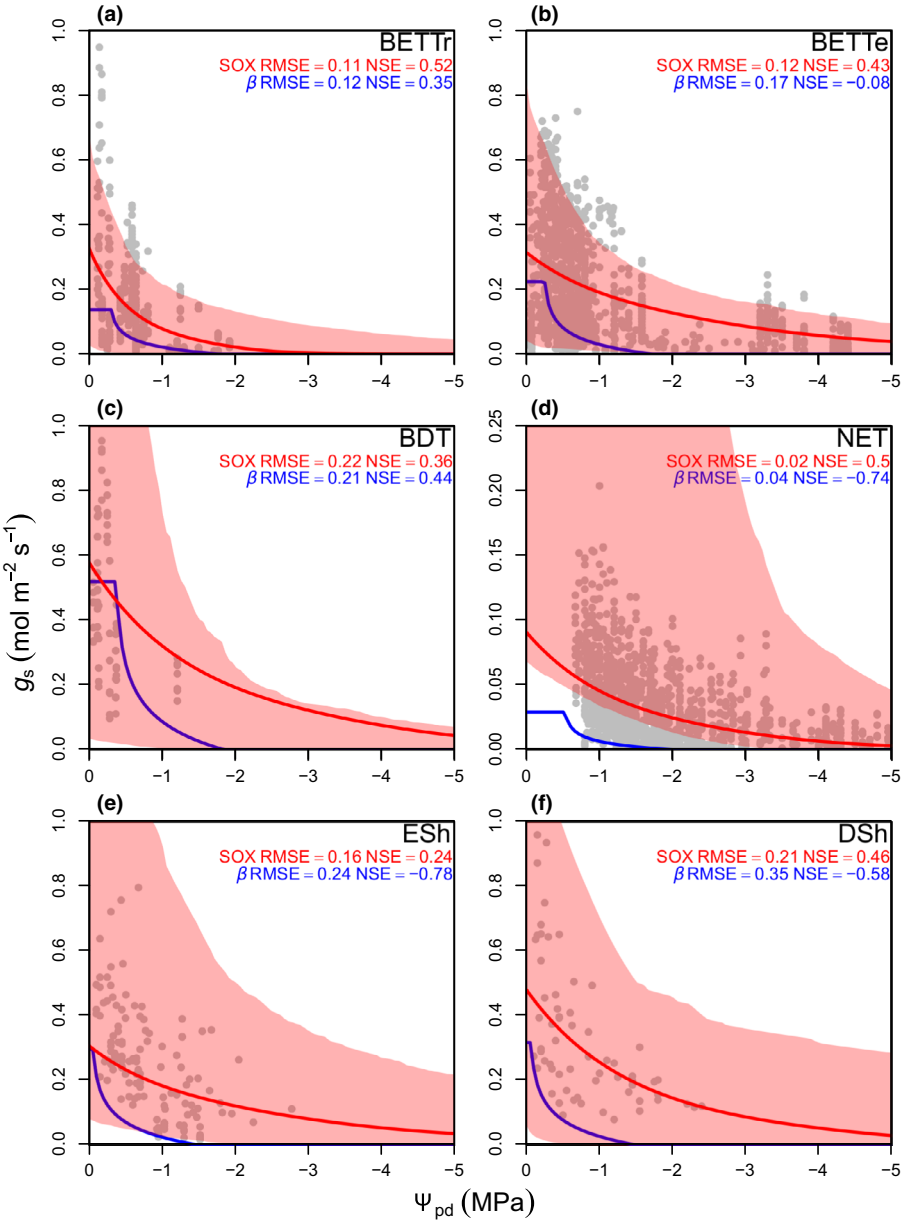

Fig. 2 Predicted and observed (grey points) stomatal conductance (g_s) response to changes in leaf predawn water potential (Ψ_{pd}) for the woody plant functional types (PFT) from Harper *et al.* (2016), except for needleleaf deciduous trees, which were not present in the dataset used in this study. The red and blue lines are the best fits from the stomatal optimization based on xylem hydraulics (SOX) and β-function (Eqns 7, 8), respectively. The shaded regions are nonparametric 95% confidence boundaries derived from 1000 bootstrapping replications of the SOX hydraulic inputs. All environmental conditions except Ψ_{pd} were held constant at their median values when the g_s measurements were taken. The Ψ_{pd} was converted in soil volumetric water content to drive the β-function using the Brooks & Corey (1964) equations parameterized with soil physical properties derived from the Met Office Central Ancillary Program (Dharssi *et al.*, 2009). The model fit to data is shown as the root-mean-square errors (RMSE) and Nash-Sutcliffe (1970) model efficiency index (NSE). The PFT abbreviations in each panel are as follows: (a) broadleaf evergreen tropical tree (BET-Tr); (b) broadleaf evergreen temperate tree (BET-Te); (c) broadleaf deciduous tree (BDT); (d) needleleaf evergreen tree (NET); (e) evergreen shrubs (ESh); and (f) deciduous shrubs (DSh).

(Fig. 5b). JULES-SOX deviation from the observed mean annual GPP was considerably smaller (71.6 g C m^{-2}; Fig. 5b). The significantly lower annual GPP predicted by default JULES can be attributed to β-function-induced GPP declines, which also produced a stronger GPP seasonality than is present in the data (Fig. 5c). JULES overestimated the median observed GPP seasonality by 70%, compared with a 13% overestimation by JULES-SOX (Fig. 5c). This difference means JULES predicts 17% of the sites have a markedly seasonal GPP with a Seasonality Index (SI; Walsh & Lawler, 1981) higher than 0.8, while just 4% of the sites actually have SI > 0.8. JULES-SOX predicts only 8% of the sites would have SI > 0.8.

The light-use efficiency (LUE; Fig. 6) is the ratio between GPP and the I_{par} absorbed by the canopy (Stocker *et al.*, 2018), and can be used to disentangle the effects of soil moisture and light availability controlling the vegetation GPP. The JULES LUE declined as soil dried out, with a mean linear slope of 1.21 (± 0.1) across all biomes. By contrast, the JULES-SOX LUE–soil moisture relationship had a mean slope of 0.73 (± 0.21), with some biomes, such as DBF, reaching a slope as low as 0.22 (Fig. 6b). The consequence of sustaining higher LUE at low soil moisture in JULES-SOX is a greater depletion of soil moisture, as indicated by the more left-skewed soil moisture probability distribution predicted by JULES-SOX (lower panels in Fig. 6). The mean moisture content of the top 1 m of soil predicted by JULES-SOX was, on average, 10% lower than default JULES. In JULES-SOX some biomes, such as ENF, could reach a soil moisture, on average, 17% lower than JULES (Fig. 6f).

Table 2 Observed (Obs) mean (± SD) hydraulic parameters compiled from the literature for each plant functional type (PFT) from JULES (Harper *et al.*, 2016).

	Ψ_{50} (MPa)			*a* (unitless)			r_{pmin} (10^{-3} mol^{-1} m^2 s MPa)		
PFT	*N*	Obs	Cal[a]	*N*[b]	Obs	Cal	*N*	Obs	Cal
BET-Tr	77	−1.9 (± 1.3)	−1.7	20	4.4 (± 2.1)	2.1	40	2.2 (± 3.4)	0.6
BET-Te	44	−2.7 (± 1.5)	−1.8	17	3.7 (± 1.8)	2.8	40	3.1 (± 8)	5
BDT	87	−2.6 (± 1.4)	−1.6	43	5.5 (± 3.8)	3.5	31	5.3 (± 5.6)	0.5
NET	48	−4.2 (± 1.2)	−2.6	25	8.7 (± 4.9)	4.9	20	2.4 (± 1.8)	4.2
NDT	5	−3.4 (± 0.6)	−1.8	2	7.4 (± 5)	1.8	2	8 (± 4.3)	9
C_3	45	−3.1 (± 1.6)	−2.4	–	–	2.2	–	–	3.2
C_4	15	−2.7 (± 1.7)	−1.5	–	–	1.8	–	–	9.5
ESh	61	−4 (± 2.2)	−2.1	53	4.1 (± 3.3)	2.5	49	1.5 (± 1.8)	9.5
DSh	26	−4 (± 2.3)	−1.8	3	3.4 (± 2.2)	2.1	4	2.6 (± 2.4)	5

BET-Tr, broadleaf evergreen tropical tree; BET-Te, broadleaf evergreen temperate tree; BDT, broadleaf deciduous tree; NET, needleleaf evergreen tree; NDT, needleleaf deciduous tree; C_3, C_3 grasses; C_4, C_4 grasses; ESh, evergreen shrubs; DSh, deciduous shrubs.
[a]The calibrated (Cal) columns are the parameter values that maximize the fit of the Joint UK Land Environment Simulator–stomatal optimization based on xylem hydraulics (JULES-SOX) to observed gross primary productivity (GPP) in the calibration sites (see Supporting Information Table S2; Fig. S2).
[b]The *N* column is the number of species compiled for the correspondent parameter.

Discussion

We report the first evaluation of a LSM using a stomatal optimization model fully based on xylem hydraulics to drive the vegetation stomatal responses to climate. Our results provide support for the SOX underlying hypothesis that stomata evolved to balance carbon assimilation with instantaneous hydraulic conductance loss. The risk of mortality through hydraulic failure (Choat *et al.*, 2012; Rowland *et al.*, 2015; Anderegg *et al.*, 2016; Adams *et al.*, 2017) should drive the evolution of mechanisms to prevent the plant from reaching lethal embolism thresholds (Sperry, 2004). There is abundant evidence that stomata controls xylem tension, and consequently embolism (Hubbard *et al.*, 2001; Brodribb *et al.*, 2003; Meinzer *et al.*, 2009; Klein, 2014). Our model represents this xylem–stomata coordination through the assumption of optimization by natural selection (Wolf *et al.*, 2016).

Whereas our model fits the observations of most PFTs better than its empirical alternative, there is still a considerable amount of unexplained variance in the data (Fig. 2). This can be partially attributed to the large hydraulic heterogeneity within each PFT, but we must also acknowledge that many processes not directly related to xylem hydraulics are important to plant life history and stomatal evolution. Processes related to nutrient use and acquisition, carbohydrate allocation and storage, the maintenance of tissues and biochemical apparatus, and protection from pathogens and herbivores (Melotto *et al.*, 2008; Cramer *et al.*, 2009; Prentice *et al.*, 2014) could all explain part of our model residual variance. It is extremely important to explore the relevance of these processes in future research on stomatal optimality. However, the SOX model as we propose it already provides a parsimonious alternative to the empirical models commonly used in LSMs.

Our findings that xylem hydraulics-based models can adequately simulate stomatal behaviour agree with other recent studies. For example, Anderegg *et al.* (2018b) shows that a hydraulics-based optimization model can simulate the stomatal behaviour of woody plants better than the CF model. More recently, Wang *et al.* (2019) shows that a similar hydraulics-based model can predict stomatal responses to increased CO_2 better than the Ball–Berry–Leuning empirical model (Leuning, 1995). These results show the potential of using plant hydraulics to model the stomatal behaviour of plants across contrasting environmental conditions, and supports its use in ESMs to project the evolution of global climate.

The analytical formulation developed for SOX facilitates its coupling to LSMs, allowing the host LSM to constrain its predictions using plant hydraulic information. We show that inclusion of plant hydraulics in JULES through SOX improves its capabilities to simulate GPP and soil moisture dynamics in most of the studied biomes (Figs 3–5). In addition, SOX opens new possibilities to evaluate LSM predictions and expands the range of hypotheses that can be tested with JULES. Using JULES-SOX within ESMs will allow us to understand how hydraulic processes affect climatic and biogeochemical cycles at the global scale, as well as to investigate the role of plant hydraulics on vegetation distribution and its response to climate change.

SOX parametrization and parsimony

Other LSMs and DGVMs have already successfully employed principles of plant hydraulics (Hickler *et al.*, 2006; Bonan *et al.*, 2014; Kennedy *et al.*, 2019), but JULES-SOX is the first LSM to use the new generation of hydraulically based stomatal optimization models (Wolf *et al.*, 2016; Sperry *et al.*, 2017; Anderegg *et al.*, 2018b; Eller *et al.*, 2018b) to predict stomatal responses to climate. The SPA (Williams *et al.*, 1996) adaptation to the community land model (CLM) by Bonan *et al.* (2014) was one of the first approaches to link plant stomatal function to plant hydraulic processes in a LSM. Despite SPA being an extremely useful model, SOX has an advantage in circumstances where assuming a strict isohydric behaviour is not appropriate (Klein, 2014; Martinez-Vilalta *et al.*, 2014). In relation to SOX, SPA does not represent dynamic changes in the plant hydraulic conductance or

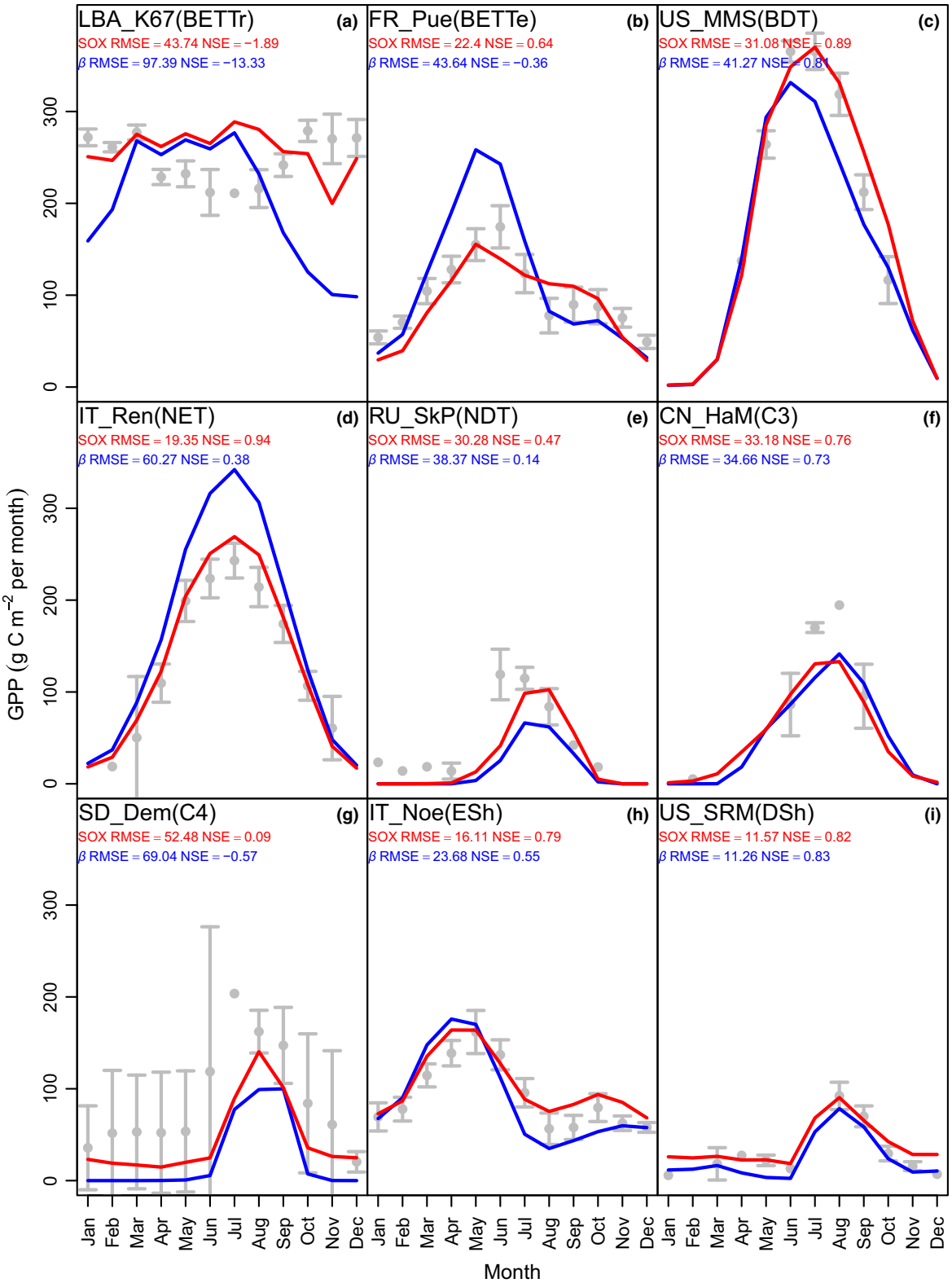

Fig. 3 Monthly mean gross primary production (GPP) modelled by default Joint UK Land Environment Simulator (JULES, blue line) and JULES-stomatal optimization based on xylem hydraulics (JULES-SOX, red line) vs observations (grey points are means and bars are 2 × SE) at each eddy flux site used for calibrating the SOX hydraulic parameters (plant functional type (PFT); Supporting Information Table S2; Fig. S3). The model fit to data is shown as the root-mean-square errors (RMSE) and Nash-Sutcliffe (1970) model efficiency index (NSE). The PFT abbreviations in each panel are as follows: (a) broadleaf evergreen tropical tree (BET-Tr); (b) broadleaf evergreen temperate tree (BET-Te); (c) broadleaf deciduous tree (BDT); (d) needleleaf evergreen tree (NET); (e) needleleaf deciduous tree (NDT); (f) C_3 grasses (C_3); (g) C_4 grasses (C_4); (h) evergreen shrubs (ESh); (i) deciduous shrubs (DSh).

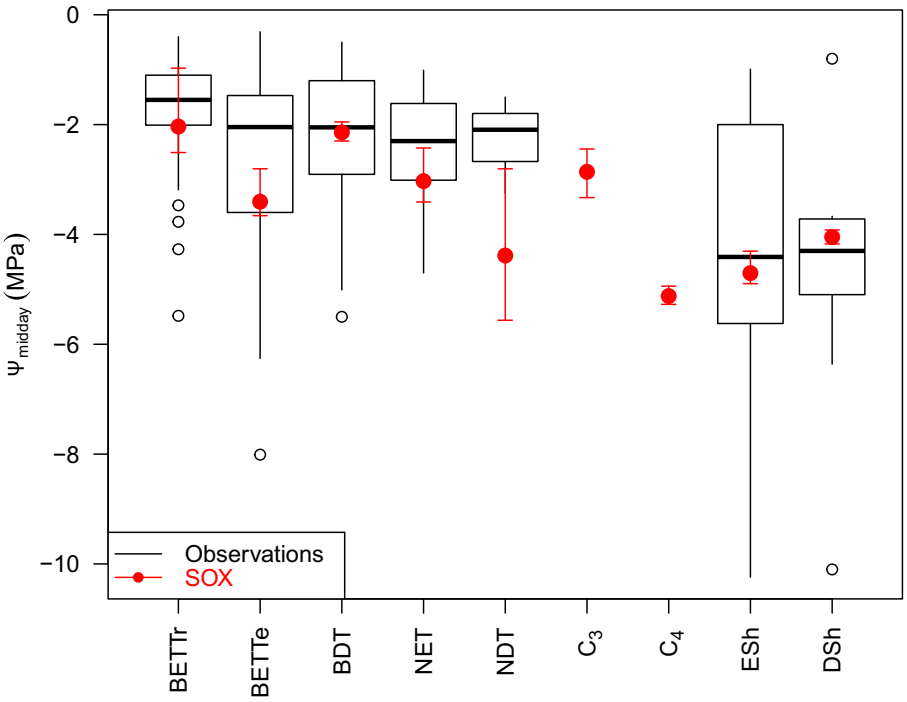

Fig. 4 Minimum observed midday leaf water potential (Ψ_{midday}) from 279 woody plant species compiled from the literature grouped using the Harper *et al.* (2016) plant functional type (PFT) categories. The Ψ_{midday} for each of the calibration sites as modelled by stomatal optimization based on xylem hydraulics (SOX) (see Supporting Information Table S2; Fig. S2) is plotted in red. The circle is the mean Ψ_{midday} and the arrows indicate the minimum and maximum Ψ_{midday}. The data for the deciduous PFT were restricted to the growing season. The PFT abbreviations in each panel are as follows: broadleaf evergreen tropical tree (BET-Tr); broadleaf evergreen temperate tree (BET-Te); broadleaf deciduous tree (BDT); needleleaf evergreen tree (NET); needleleaf deciduous tree (NDT); C_3 grasses (C_3); (g) C_4 grasses (C_4); evergreen shrubs (ESh); deciduous shrubs (DSh).

Table 3 Median Nash-Sutcliffe (1970) model efficiency index (NSE) and root-mean-square error (RMSE) for the biomes used for evaluating the Joint UK Land Environment Simulator–stomatal optimization based on xylem hydraulics (JULES-SOX) and the default JULES.

		JULES-SOX		JULES	
Biome[a]	*N*[b]	NSE	RMSE	NSE	RMSE
CRO	3	0.49	123.12	0.57	141.1
DBF	7	0.89	37.32	0.83	47.19
DNF	1	0.58	25.93	0.37	31.97
EBF-Te	3	−0.23	45.22	−1.24	66.36
EBF-Tr	6	0.41	40.36	−2.77	73.53
ENF	5	0.9	34.14	0.59	40.58
GRA	12	0.22	32.31	−0.01	30.62
MF	3	0.85	47.87	0.59	79.29
SAV	5	−0.4	59.72	−2.12	89.69
SHR	4	0.78	14.90	0.64	15.92
WET	21	0.68	32.23	0.46	38.67

[a]Biome abbreviations are as follows: CRO, cropland; DBF, deciduous broadleaf forests; DNF, deciduous needleleaf forests; EBF-Te, temperate evergreen broadleaf forests; EBF-Tr, tropical evergreen broadleaf forests; ENF, evergreen needleleaf forest; GRA, grassland; MF, mixed forest; SAV, savannah; SHR, shrubland; WET, wetlands.
[b]The *N* column is the number of sites representing the biome in the eddy covariance dataset.

an anisohydric mode of stomatal regulation (Williams *et al.*, 1996; Fisher *et al.*, 2006). However, SPA accounts for plant hydraulic capacitance, which can be important for plant functioning, especially during the early morning (Goldstein *et al.*, 1998), and is currently not implemented in SOX.

Recently, Kennedy *et al.* (2019) implemented a plant hydraulic scheme (PHS) in a CLM. The PHS simulates dynamic changes in hydraulic conductance in different compartments along the soil–atmosphere continuum, providing a more detailed representation than SOX of hydraulic processes occurring along the soil–plant hydraulic pathway. However, PHS still requires empirical parameters to represent stomatal responses to soil drought and *D* (Kennedy *et al.*, 2019), namely the g_0 and g_1 parameters from the Medlyn *et al.* (2011) model, and the critical and wilting points used in the empirical stress factor. The main advantage of SOX is providing an alternative to the β-function and empirical stomatal parameters by linking plant hydraulic processes directly to stomatal functioning. As we treat the soil–plant–atmosphere pathway as a single hydraulic compartment, SOX only requires the hydraulic parameters r_{pmin}, Ψ_{50} and a to predict stomatal responses to climate. This makes SOX even more parsimonious than default JULES, which requires four empirical parameters to simulate stomatal responses to climate (Eqns 7, 8) and does not simulate any aspect of vegetation hydraulic functioning (Clark *et al.*, 2011).

We show that the SOX hydraulic parameters in most PFTs can be constrained with plant branch-level hydraulic observations (Table 2), which is an advantage over models that employ empirical parameters difficult to constrain and interpret biologically. However, we observed discrepancies between the SOX-calibrated parameters and the observed hydraulic traits in certain PFTs (Table 2). In some cases, such as NDT, the parameter discrepancy may have been a result of a very restricted observational sampling of hydraulic parameters in this group. The NDT only had Ψ_{50} data for five species and a and r_{pmin} for two species (Table 2). Considering that the observations used in this study were not collected in the same FLUXNET sites used to evaluate SOX, some of the observed discrepancies between calibrated and measured parameters might reflect hydraulic differences between

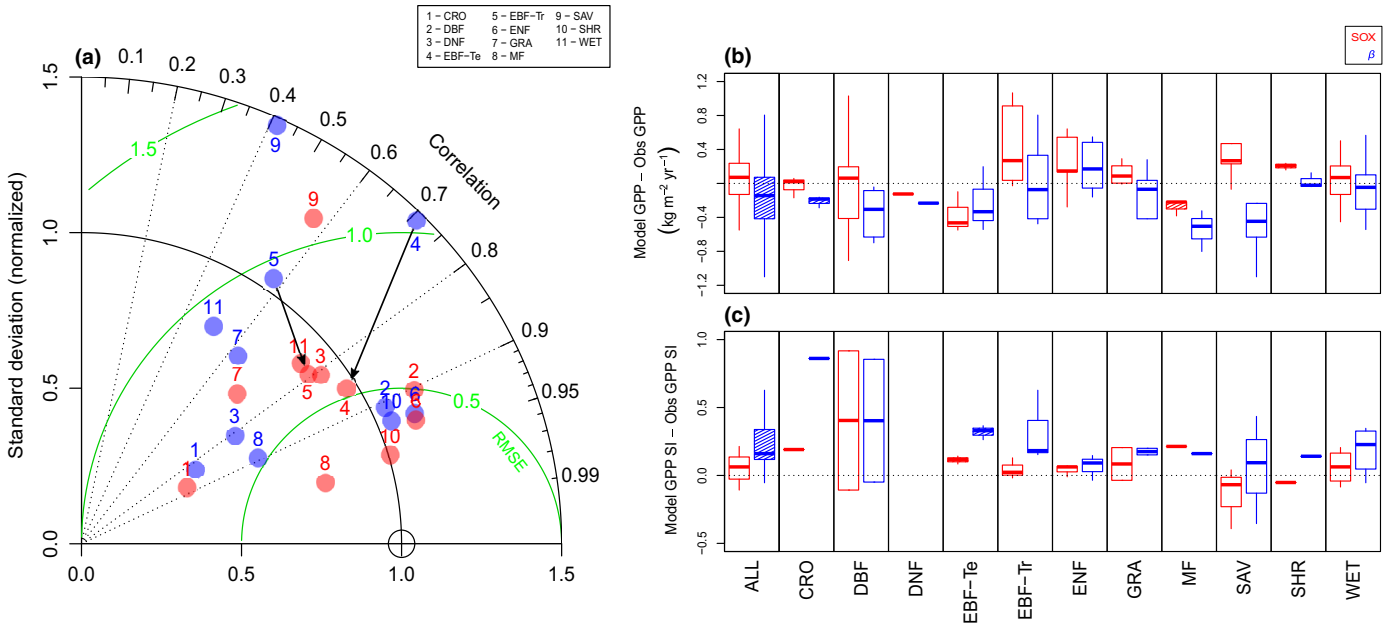

Fig. 5 (a) The Taylor diagram shows the difference in Joint UK Land Environment Simulator (JULES) and JULES-stomatal optimization based on xylem hydraulics (JULES-SOX) skill to predict the monthly gross primary productivity (GPP) in each studied biome. Green lines are the model-centred root-mean-square errors (RMSE), and points closer to the reference circle on the *x*-axis indicate higher model skill. The two arrows highlight the improvement in model skill for tropical evergreen broadleaf forests (EBF-Tr) and temperate evergreen broadleaf forests (EBF-Te). The boxplot panels show the differences between models (default JULES in blue, JULES-SOX in red) and observations (Obs) in the annual GPP (b) and the GPP seasonality (GPP SI) (c). Data gaps were excluded from the annual GPP calculations for both models and observations, and therefore the differences can be used to evaluate the model skill, but the absolute values do not represent the total annual GPP in each biome. The GPP SI was computed using the approach from Walsh & Lawler (1981). Boxes filled with lines are different (at $\alpha = 0.05$) from 0 in a one-sample *t*-test. The biomes are abbreviated as follows: cropland (CRO); deciduous broadleaf forests (DBF); deciduous needleleaf forests (DNF); temperate evergreen broadleaf forests (EBF-Te); tropical evergreen broadleaf forests (EBF-Tr); evergreen needleleaf forest (ENF); grassland (GRA); mixed forest (MF); savannah (SAV); shrubland (SHR); and wetlands (WET).

populations treated as the same PFT in this study. For example, the deciduous angiosperms species present in the XFT dataset used in this study contain mostly hydraulic data from cold-deciduous temperate species (Mencuccini *et al.*, 2019b), which might not be adequate to describe the hydraulic system of tropical and subtropical drought-deciduous. Our hydraulic scheme opens up possibilities of improving the representation of different global vegetation types in JULES with different hydraulic and phenological strategies. Capturing the large diversity of ecological strategies in plants is important to simulate species-rich ecosystems such as tropical forests (Xu *et al.*, 2016).

Anderegg *et al.* (2018a) computed the community-weighted average values for Ψ_{50} in two of the FLUXNET sites used in this study (US-MMS and IT-Ren) and obtained values closer to the calibrated values for BDT and NET (−2.1 and −3.6 MPa, respectively) than the means from our compiled hydraulic dataset (Table 2). In Eller *et al.* (2018b) a numerical version of SOX outperformed the β-function approach when parameterized with locally measured branch-level hydraulic data from EBF-Tr. These findings suggest that SOX can be constrained with *in situ* hydraulic measurements when these are available. However, we must also consider the possibility that there are intrinsic limitations in using branch-level hydraulic data to parameterize the model. Roots and leaves can be more vulnerable to embolism than branches (Bartlett *et al.*, 2016; Wolfe *et al.*, 2016), which can make these tissues bottleneck plant hydraulic conductance during drought. The soil outside the roots can also limit plant hydraulic conductance and, ultimately, control its water use (Fisher *et al.*, 2007). These bottlenecks could bias the SOX-calibrated hydraulic parameters towards the limiting component and explain its departure from the branch-level hydraulic data. In this case, SOX parameterization would benefit from the use of more integrative methodologies to estimate hydraulic parameters that represent the entire soil–plant hydraulic vulnerability (Eller *et al.*, 2018a). Alternatively, the SOX structure (i.e. the *K* function in Eqn 2) would need to explicitly represent the variability between different hydraulic compartments along the soil–plant–atmosphere pathway, similar to SPA or other models (Eller *et al.*, 2018b; Kennedy *et al.*, 2019; Mencuccini *et al.*, 2019b).

Ecosystem-level implications of SOX

Stomatal optimization based on xylem hydraulics improved JULES GPP simulation in over 70% of the 70 studied sites, and soil moisture dynamics in 80% of the 10 sites where soil moisture data were available. This improved fit was achieved using hydraulic parameters calibrated against the GPP data of a small subset of eddy flux sites (the sites in Fig. S2), which suggests that the calibrated parameters are generic enough to be used in global simulations. The lower sensitivity of SOX to soil moisture improved the simulations of annual GPP (Fig. 5) and predicted terrestrial biomes to assimilate on average 2.58 Mg C ha^{-1} yr^{-1} or 30% more than predicted by default JULES. This increased carbon assimilation could affect Earth's atmospheric CO_2

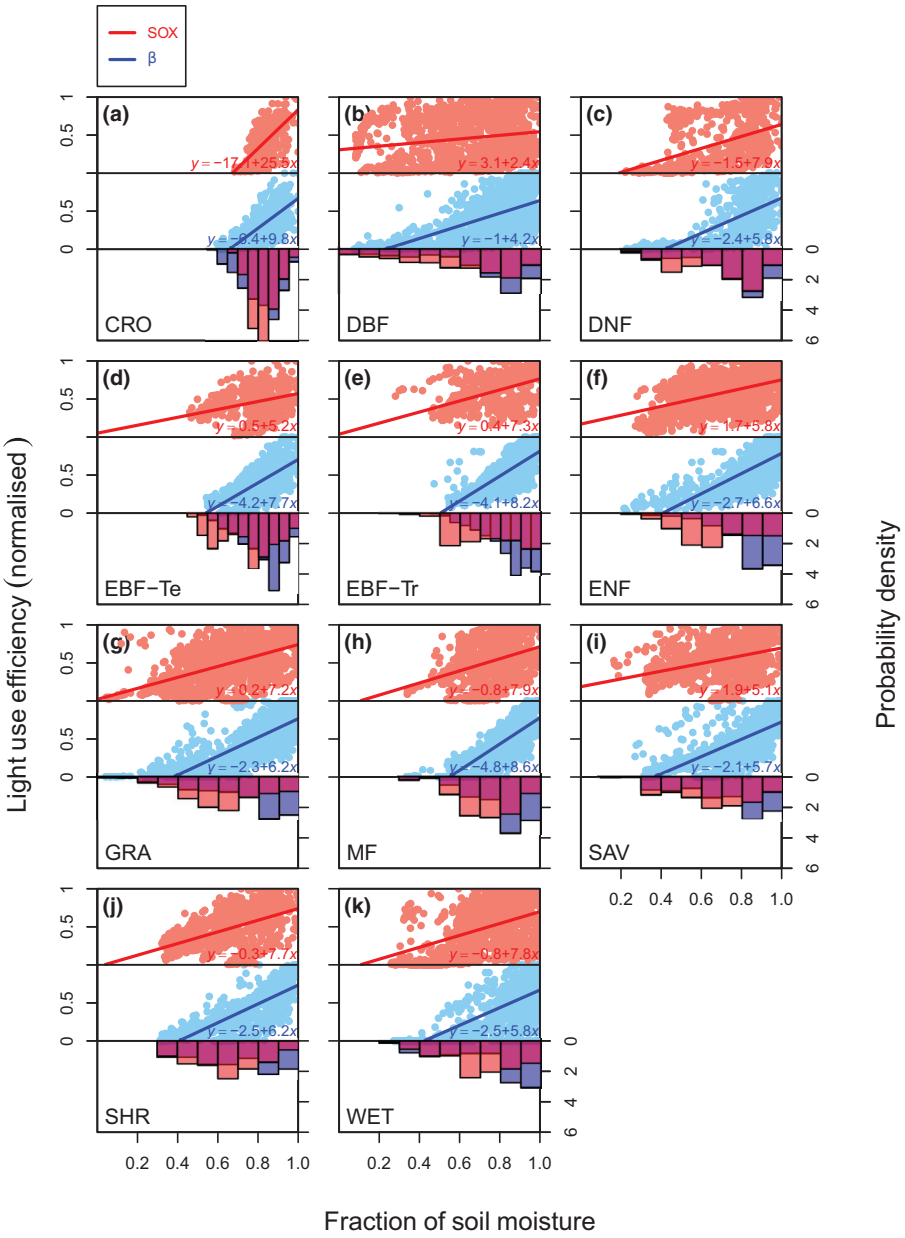

Fig. 6 Model predictions of the normalized light-use efficiency responses to soil moisture, expressed as a fraction of the soil moisture saturation point at the top 1 m of soil. The light use efficiency is the ratio between gross primary productivity and the photosynthetic active radiation absorbed by the canopy. The default JULES predictions are in blue and JULES-SOX predictions in red. The lines in the scatter plot panels are linear regressions fit to the data. The histograms on the bottom panels are the soil moisture probability density predicted by each model. The biomes are abbreviated as follows: (a) cropland (CRO); (b) deciduous broadleaf forests (DBF); (c) deciduous needleleaf forests (DNF); (d) temperate evergreen broadleaf forests (EBF-Te); (e) tropical evergreen broadleaf forests (EBF-Tr); (f) evergreen needleleaf forest (ENF); (g) grassland (GRA); (h) mixed forest (MF); (i) savannah (SAV); (j) shrubland (SHR); and (k) wetlands (WET).

evolution and climate change projections (Cox *et al.*, 2000; Winkler *et al.*, 2019).

The JULES-SOX model particularly improved the fit of EBF-Tr sites to the observations (Fig. 5; Table 3), using hydraulic parameters very similar to those observed in BET-Tr (Table 2). Considering that SOX is also able to capture the response of EBF-Tr even to extreme experimental drought (Eller *et al.*, 2018b), JULES-SOX may contribute to decrease the large uncertainty in how these important ecosystems will respond to climate change (Sitch *et al.*, 2008). Tropical forest productivity estimated by SOX is less sensitive to seasonal soil drought (Figs 3, S4), which is consistent with the little seasonality often observed in tropical forest–atmosphere CO_2 exchange (Grace *et al.*, 1995; Carswell *et al.*, 2002; Alden *et al.*, 2016), as well as to forest responses to experimental drought (Meir *et al.*, 2009; da Costa *et al.*, 2010; Meir *et al.*, 2018). da Costa *et al.* (2018) showed that even after 15 yr of partial rainfall exclusion, Amazon trees can maintain or even increase their transpiration rates (albeit following significant mortality). Whereas tropical forest resistance to drought has previously been attributed only to deep roots possessed by the vegetation (Nepstad *et al.*, 1994), our results indicate that plants more resistant to embolism could maintain their carbon assimilation during drought even without a deeper root system.

The unavoidable consequence of maintaining stomatal gas exchange during soil drought is a greater depletion of soil moisture reserves (Figs 6, S4, S7). This behaviour is a direct consequence of the main assumption in SOX, which reflects a 'use or lose it' stomatal regulation strategy with respect to soil moisture (Sperry *et al.*, 2017). SOX assumes plants with a more

conservative water-use strategy will be outcompeted by neighbouring plants with a less conservative stomatal behaviour (Wolf *et al.*, 2016). The demographic consequences of the stomatal regulation strategy embedded in SOX should be explored in future studies using the dynamic vegetation component of JULES (Cox, 2001; Moore *et al.*, 2018). The more competitive soil moisture dynamics predicted by SOX, together with a more accurate representation of vegetation drought-induced mortality, which also can be developed from SOX, might be the key to predicting sudden and widespread vegetation die-off during droughts that have been increasingly reported in ecosystems around the globe (Allen *et al.*, 2010; Worrall *et al.*, 2010; Meir *et al.*, 2015).

Acknowledgements

This research was supported by the Newton Fund through the Met Office Climate Science for Service Partnership Brazil (CSSP Brazil) and an NERC independent fellowship grant NE/N014022/1 to LR. This work used eddy covariance data acquired and shared by the FLUXNET community, including the following networks: AmeriFlux, AfriFlux, AsiaFlux, CarboAfrica, CarboEuropeIP, CarboItaly, CarboMont, ChinaFlux, Fluxnet-Canada, GreenGrass, ICOS, KoFlux, LBA, NECC, OzFlux-TERN, TCOS-Siberia, and USCCC. The ERA-Interim reanalysis data were provided by ECMWF and processed by LSCE. The FLUXNET eddy covariance data processing and harmonization were carried out by the European Fluxes Database Cluster, AmeriFlux Management Project, and Fluxdata project of FLUXNET, with the support of CDIAC and ICOS Ecosystem Thematic Center, and the OzFlux, ChinaFlux and AsiaFlux offices.

Author contributions

CBE, LR, MM, SS and PMC led the scientific development of SOX. PMC and CBE derived the analytical solution. CBE evaluated leaf-level SOX using data provided by LR, PM, MM, TR, BEM, YW, TK, GST, RSO, ISM, BHPR. CBE and KW coded SOX into JULES. KW and AH created a JULES suite used by CBE to evaluate JULES-SOX against eddy covariance data collected by KF, GW, LM, among other FLUXNET and LBA PIs. All authors contributed to writing the manuscript.

ORCID

Peter M. Cox https://orcid.org/0000-0002-0679-2219
Cleiton B. Eller https://orcid.org/0000-0002-7795-2574
Kathrin Fuchs https://orcid.org/0000-0003-1776-283X
Anna Harper https://orcid.org/0000-0001-7294-6039
Tamir Klein https://orcid.org/0000-0002-3882-8845
Ilaine S. Matos https://orcid.org/0000-0001-5557-5133
Belinda E. Medlyn https://orcid.org/0000-0001-5728-9827
Patrick Meir https://orcid.org/0000-0002-2362-0398
Leonardo Montagnani https://orcid.org/0000-0003-4412-4243
Maurizio Mencuccini https://orcid.org/0000-0003-0840-1477
Rafael S. Oliveira https://orcid.org/0000-0002-6392-2526
Bruno H. P. Rosado https://orcid.org/0000-0002-8924-8672
Teresa Rosas https://orcid.org/0000-0002-8734-9752
Lucy Rowland https://orcid.org/0000-0002-0774-3216
Stephen Sitch https://orcid.org/0000-0003-1821-8561
Grazielle S. Teodoro https://orcid.org/0000-0002-5528-8828
Yael Wagner https://orcid.org/0000-0002-2588-9278
Karina Williams https://orcid.org/0000-0002-1185-535X
Georg Wohlfahrt https://orcid.org/0000-0003-3080-6702

References

Adams HD, Zeppel MJB, Anderegg WRL, Hartmann H, Landhäusser SM, Tissue DT, Huxman TE, Hudson PJ, Franz TE, Allen CD *et al.* 2017. A multi-species synthesis of physiological mechanisms in drought-induced tree mortality. *Nature Ecology and Evolution* **1**: 1285–1291.

Alden CB, Miller JB, Gatti LV, Gloor MM, Guan K, Michalak AM, van der Laan-Luijkx IT, Touma D, Andrews A, Basso LS *et al.* 2016. Regional atmospheric CO_2 inversion reveals seasonal and geographic differences in Amazon net biome exchange. *Global change biology* **22**: 3427–3443.

Allen CD, Macalady AK, Chenchouni H, Bachelet D, McDowell N, Vennetier M, Kitzberger T, Rigling A, Breshears DD, Hogg EH *et al.* 2010. A global overview of drought and heat-induced tree mortality reveals emerging climate change risks for forests. *Forest Ecology and Management* **259**: 660–684.

Anderegg WRL, Klein T, Bartlett M, Sack L, Pellegrini AFA, Choat B, Jansen S. 2016. Meta-analysis reveals that hydraulic traits explain cross-species patterns of drought-induced tree mortality across the globe. *Proceedings of the National Academy of Sciences, USA* **113**: 5024–5029.

Anderegg WRL, Konings AG, Trugman AT, Yu K, Bowling DR, Gabbitas R, Karp DS, Pacala S, Sperry JS, Sulman BN *et al.* 2018a. Hydraulic diversity of forests regulates ecosystem resilience during drought. *Nature* **561**: 538.

Anderegg WRL, Wolf A, Arango-Velez A, Choat B, Chmura DJ, Jansen S, Kolb T, Li S, Meinzer FC, Pita P *et al.* 2018b. Woody plants optimise stomatal behaviour relative to hydraulic risk. *Ecology Letters* **21**: 968–977.

Baldocchi D, Falge E, Gu L, Olson R, Hollinger D, Running S, Anthoni P, Bernhofer C, Davis K, Evans R *et al.* 2001. FLUXNET: a new tool to study the temporal and spatial variability of ecosystem-scale carbon dioxide, water vapor, and energy flux densities. *Bulletin of the American Meteorological Society* **82**: 2415–2434.

Bartlett MK, Klein T, Jansen S, Choat B, Sack L. 2016. The correlations and sequence of plant stomatal, hydraulic, and wilting responses to drought. *Proceedings of the National Academy of Sciences, USA* **113**: 13098–13103.

Berninger F, Hari P. 1993. Optimal regulation of gas exchange: evidence from field data. *Annals of Botany* **71**: 135–140.

Best MJ, Pryor M, Clark DB, Rooney GG, Essery R, Ménard CB, Edwards JM, Hendry MA, Porson A, Gedney N. 2011. The Joint UK Land Environment Simulator (JULES), model description–Part 1: energy and water fluxes. *Geoscientific Model Development* **4**: 677–699.

Bonan GB, Williams M, Fisher RA, Oleson KW. 2014. Modeling stomatal conductance in the earth system: linking leaf water-use efficiency and water transport along the soil-plant-atmosphere continuum. *Geoscientific Model Development* **7**: 2193–2222.

Bozdogan H. 1987. Model selection and Akaike's Information Criterion (AIC): the general theory and its analytical extensions. *Psychometrika* **52**: 345–370.

Brodribb TJ, Holbrook NM, Edwards EJ, Gutiérrez MV. 2003. Relations between stomatal closure, leaf turgor and xylem vulnerability in eight tropical dry forest trees. *Plant, Cell & Environment* **26**: 443–450.

Brooks R, Corey T. 1964. Hydraulic properties of porous media. *Hydrology Papers*, Colorado State University **24**: 37.

Buckley TN. 2017. Modeling stomatal conductance. *Plant Physiology* **174**: 572–582.

Buckley TN. 2019. How do stomata respond to water status? *New Phytologist* **224**: 21–36.

Carswell FE, Costa AL, Palheta M, Malhi Y, Meir P, Costa JDPR, Ruivo MDL, Leal LDSM, Costa JMN, Clement RJ *et al.* 2002. Seasonality in CO_2 and H_2O flux at an eastern Amazonian rain forest. *Journal of Geophysical Research D: Atmospheres* **107**: LBA-43.

Choat B, Jansen S, Brodribb TJ, Cochard H, Delzon S, Bhaskar R, Bucci SJ, Feild TS, Gleason SM, Hacke UG *et al.* 2012. Global convergence in the vulnerability of forests to drought. *Nature* **491**: 752–755.

Christoffersen BO, Gloor M, Fauset S, Fyllas NM, Galbraith DR, Baker TR, Kruijt B, Rowland L, Fisher RA, Binks OJ *et al.* 2016. Linking hydraulic traits to tropical forest function in a size-structured and trait-driven model (TFS v.1-Hydro). *Geoscientific Model Development* **9**: 1–29.

Clark DB, Mercado LM, Sitch S, Jones CD, Gedney N, Best MJ, Pryor M, Rooney GG, Essery RLH, Blyth E *et al.* 2011. The Joint UK Land Environment Simulator (JULES), model description – Part 2: carbon fluxes and vegetation. *Geoscientific Model Development Discussions* **4**: 641–688.

Collatz GJ, Ball JT, Grivet C, Berry JA. 1991. Physiological and environmental regulation of stomatal conductance, photosynthesis and transpiration: a model that includes a laminar boundary layer. *Agricultural and Forest meteorology* **54**: 107–136.

Collatz GJ, Ribas-Carbo M, Berry JA. 1992. Coupled photosynthesis-stomatal conductance model for leaves of C_4 plants. *Functional Plant Biology.* **19**: 519–538.

Cosby BJ, Hornberger GM, Clapp RB, Ginn TR. 1984. A statistical exploration of the relationships of soil moisture characteristics to the physical properties of soils. *Water Resources Research* **20**: 682–690.

Cowan IR. 1986. Economics of carbon fixation in higher plants. In: Givnish TJ, ed. *On the economy of plant form and function.* Cambridge, UK: Cambridge University Press, 133–170.

Cowan I. 2002. Fit, fitter, fittest; where does optimisation fit in? *Silva Fennica* **36**: 745–754.

Cowan IR, Farquhar GD. 1977. Stomatal function in relation to leaf metabolism and environment. *Symposia of the Society for Experimental Biology* **31**: 471–505.

Cox PM. 2001. *Description of the "TRIFFID" Dynamic Global Vegetation Model.* Hadley Centre technical note 24. Bracknell, UK: Met Office.

Cox PM, Betts RA, Jones CD, Spall SA, Totterdell IJ. 2000. Acceleration of global warming due to carbon-cycle feedbacks in a coupled climate model. *Nature* **408**: 184.

Cox PM, Huntingford C, Harding RJ. 1998. A canopy conductance and photosynthesis model for use in a GCM land surface scheme. *Journal of Hydrology* **212–213**: 79–94.

Cramer MD, Hawkins HJ, Verboom GA. 2009. The importance of nutritional regulation of plant water flux. *Oecologia* **161**: 15–24.

da Costa ACL, Galbraith D, Almeida S, Portela BTT, da Costa M, de Athaydes Silva Junior J, Braga AP, de Gonçalves PHL, de Oliveira AA, Fisher R *et al.* 2010. Effect of 7 yr of experimental drought on vegetation dynamics and biomass storage of an eastern Amazonian rainforest. *New Phytologist* **187**: 579–591.

da Costa ACL, Rowland L, Oliveira RS, Oliveira AAR, Binks OJ, Salmon Y, Vasconcelos SS, Junior JAS, Ferreira LV, Poyatos R *et al.* 2018. Stand dynamics modulate water cycling and mortality risk in droughted tropical forest. *Global Change Biology* **24**: 249–258.

Dewar RC, Franklin O, Mäkelä A, McMurtrie RE, Valentine HT. 2009. Optimal function explains forest responses to global change. *BioScience* **59**: 127–139.

Dewar R, Mauranen A, Mäkelä A, Hölttä T, Medlyn B, Vesala T. 2018. New insights into the covariation of stomatal, mesophyll and hydraulic conductances from optimization models incorporating nonstomatal limitations to photosynthesis. *New Phytologist* **217**: 571–585.

Dharssi I, Vidale PL, Verhoef A, Macpherson B, Jones C, Best M. (2009). *New soil physical properties implemented in the Unified Model at PS18.* Met Office technical report 528. Exeter, UK: Met Office.

Duffy PB, Brando P, Asner GP, Field CB. 2015. Projections of future meteorological drought and wet periods in the Amazon. *Proceedings of the National Academy of Sciences, USA* **112**: 13172–13177.

Eller CB, Bittencourt PRL, Oliveira RS. 2018a. Using sap flow to measure whole-tree hydraulic conductance loss in response to drought. *Acta Horticulturae* **1222**: 75–84.

Eller CB, Rowland L, Oliveira RS, Bittencourt PRL, Barros FV, da Costa ACL, Meir P, Friend AD, Mencuccini M, Sitch S *et al.* 2018b. Modelling tropical forest responses to drought and El Niño with a stomatal optimization model based on xylem hydraulics. *Philosophical transactions of the Royal Society of London. Series B: Biological sciences* **373**: 20170315.

Farquhar G, Schulze E, Kuppers M. 1980. Responses to humidity by stomata of *Nicotiana glauca* L. and *Corylus avellana* L. are consistent with the optimization of carbon dioxide uptake with respect to water loss. *Australian Journal of Plant Physiology* **7**: 315–327.

Fisher RA, Williams M, Da Costa AL, Malhi Y, Da Costa RF, Almeida S, Meir P. 2007. The response of an Eastern Amazonian rain forest to drought stress: results and modelling analyses from a throughfall exclusion experiment. *Global Change Biology* **13**: 2361–2378.

Fisher RA, Williams M, Do Vale RL, Da Costa AL, Meir P. 2006. Evidence from Amazonian forests is consistent with isohydric control of leaf water potential. *Plant, Cell & Environment* **20**: 151–165.

Friend AD. 1995. PGEN: an integrated model of leaf photosynthesis, and conductance. *Ecological Modelling* **77**: 233–255.

Friend AD, Cox PM. 1995. Modelling the effects of atmospheric CO_2 on vegetation–atmosphere interactions. *Agricultural and Forest Meteorology* **73**: 295.

Goldstein G, Andrade JL, Meinzer FC, Holbrook NM, Cavelier J, Jackson P, Celis A. 1998. Stem water storage and diurnal patterns of water use in tropical forest canopy trees. *Plant, Cell & Environment* **21**: 397–406.

Grace J, Lloyd J, McIntyre J, Miranda AC, Meir P, Miranda HS, Nobre C, Moncrieff J, Massheder J, Malhi Y *et al.* 1995. Carbon dioxide uptake by an undisturbed tropical rain forest in Southwest Amazonia, 1992 to 1993. *Science* **270**: 778–780.

Harper AB, Cox PM, Friedlingstein P, Wiltshire AJ, Jones CD, Sitch S, Mercado LM, Groenendijk M, Robertson E, Kattge J *et al.* 2016. Improved representation of plant functional types and physiology in the Joint UK Land Environment Simulator (JULES v4.2) using plant trait information. *Geoscientific Model Development* **9**: 2415–2440.

Hickler T, Prentice IC, Smith B, Sykes MT, Zaehle S. 2006. Implementing plant hydraulic architecture within the LPJ Dynamic Global Vegetation Model. *Global Ecology and Biogeography* **15**: 567–577.

Hubbard RM, Ryan MG, Stiller V, Sperry JS. 2001. Stomatal conductance and photosynthesis vary linearly with plant hydraulic conductance in ponderosa pine. *Plant, Cell & Environment* **24**: 113–121.

Jacobs C. 1994. *Direct impact of atmospheric CO_2 enrichment on regional transpiration.* PhD thesis, Wageningen Agricultural University, Wageningen, the Netherlands.

Kattge J, Díaz S, Lavorel S, Prentice IC, Leadley P, Bönisch G, Garnier E, Westoby M, Reich PB, Wright IJ *et al.* 2011. TRY – a global database of plant traits. *Global Change Biology* **17**: 2905–2935.

Kennedy D, Swenson S, Oleson KW, Lawrence DM, Fisher R, da Costa ACL, Gentine P. 2019. Implementing plant hydraulics in the Community Land Model, version 5. *Journal of Advances in Modeling Earth Systems* **11**: 485–513.

Klein T. 2014. The variability of stomatal sensitivity to leaf water potential across tree species indicates a continuum between isohydric and anisohydric behaviours. *Functional Ecology* **28**: 1313–1320.

Lens F, Picon-Cochard C, Delmas CEL, Signarbieux C, Buttler A, Cochard H, Jansen S, Chauvin T, Doria LC, Del Arco M *et al.* 2016. Herbaceous angiosperms are not more vulnerable to drought-induced embolism than angiosperm trees. *Plant Physiology* **172**: 661–667.

Leuning R. 1995. A critical appraisal of a combined stomatal - photosynthesis model for C_3 plants. *Plant, Cell & Environment* **18**: 339–355.

Lin Y, Medlyn B, Duursma R. 2015. Optimal stomatal behaviour around the world. *Nature Climate Change* **5**: 459.

Loveland TR, Reed BC, Ohlen DO, Brown JF, Zhu Z, Yang L, Merchant JW. 2000. Development of a global land cover characteristics database and IGBP DISCover from 1 km AVHRR data. *International Journal of Remote Sensing* **21**: 1303–1330.

Mäkelä A, Berninger F, Hari P. 1996. Optimal control of gas exchange during drought: theoretical analysis. *Annals of Botany* **77**: 461–468.

Manzoni S, Vico G, Palmroth S, Porporato A, Katul G. 2013. Optimization of stomatal conductance for maximum carbon gain under dynamic soil moisture. *Advances in Water Resources* **62**: 90–105.

Marengo JA, Souza CM, Thonicke K, Burton C, Halladay K, Betts RA, Alves LM, Soares WR. 2018. Changes in climate and land use over the Amazon region: current and future variability and trends. *Frontiers in Earth Science* **6**: 228.

Martinez-Vilalta J, Poyatos R, Aguade D, Retana J, Mencuccini M. 2014. A new look at water transport regulation in plants. *New Phytologist* **204**: 105–115.

Medlyn BE, Barton CVM, Broadmeadow MSJ, Ceulemans R, De Angelis P, Forstreuter M, Freeman M, Jackson SB, Kellomäki S, Laitat E *et al.* 2001. Stomatal conductance of forest species after long-term exposure to elevated CO_2 concentration: a synthesis. *New Phytologist* **149**: 247–264.

Medlyn BE, De Kauwe MG, Zaehle S, Walker AP, Duursma RA, Luus K, Mishurov M, Pak B, Smith B, Wang YP *et al.* 2016. Using models to guide field experiments: a priori predictions for the CO_2 response of a nutrient- and water-limited native Eucalypt woodland. *Global Change Biology* **22**: 2834–2851.

Medlyn BE, Duursma RA, Eamus D, Ellsworth DS, Prentice IC, Barton CVM, Crous KY, De Angelis P, Freeman M, Wingate L. 2011. Reconciling the optimal and empirical approaches to modelling stomatal conductance. *Global Change Biology* **17**: 2134–2144.

Medlyn BE, Zaehle S, De Kauwe MG, Walker AP, Dietze MC, Hanson PJ, Hickler T, Jain AK, Luo Y, Parton W *et al.* 2015. Using ecosystem experiments to improve vegetation models. *Nature Climate Change* **5**: 528.

Meinzer FC, Johnson DM, Lachenbruch B, McCulloh KA, Woodruff DR. 2009. Xylem hydraulic safety margins in woody plants: coordination of stomatal control of xylem tension with hydraulic capacitance. *Functional Ecology* **23**: 922–930.

Meir P, Brando PM, Nepstad D, Vasconcelos S, Costa ACL, Davidson E, Almeida S, Fisher RA, Sotta ED, Zarin D *et al.* 2009. The effect of drought on Amazonian rain forests. In: Gash J, Keller M, Bustamante M, Silva Dias P, eds. *Amazonia and global change*. Washigton, DC, USA: American Geophysical Union, 429–449.

Meir P, Mencuccini M, Binks O, da Costa AL, Ferreira L, Rowland L. 2018. Short-term effects of drought on tropical forest do not fully predict impacts of repeated or long-term drought: gas exchange versus growth. *Philosophical Transactions of the Royal Society of London. Series B: Biological Sciences* **373**: 20170311.

Meir P, Wood TE, Galbraith DR, Brando PM, Da Costa ACL, Rowland L, Ferreira LV. 2015. Threshold responses to soil moisture deficit by trees and soil in tropical rain forests: insights from field experiments. *BioScience* **65**: 882–892.

Melotto M, Underwood W, He SY. 2008. Role of stomata in plant innate immunity and foliar bacterial diseases. *Annual Review of Phytopathology* **46**: 101–122.

Mencuccini M, Manzoni S, Christoffersen B. 2019a. Modelling water fluxes in plants: from tissues to biosphere. *New Phytologist* **222**: 1207–1222.

Mencuccini M, Rosas T, Rowland L, Choat B, Cornelissen JHC, Jansen S, Kramer K, Lepenas A, Manzoni S, Niinemets U *et al.* 2019b. Leaf economics and xylem hydraulics drive leaf/wood area ratios. *New Phytologist* **224**: 1544–1556.

Mercado LM, Bellouin N, Sitch S, Boucher O, Huntingford C, Wild M, Cox PM. 2009. Impact of changes in diffuse radiation on the global land carbon sink. *Nature* **458**: 1014.

Mercado LM, Huntingford C, Gash JHC, Cox PM, Jogireddy V. 2007. Improving the representation of radiation interception and photosynthesis for climate model applications. *Tellus, Series B: Chemical and Physical Meteorology* **59**: 553–565.

Moore JR, Zhu K, Huntingford C, Cox PM. 2018. Equilibrium forest demography explains the distribution of tree sizes across North America. *Environmental Research Letters* **13**: 084019.

Mott KA. 1988. Do stomata respond to CO_2 concentrations other than intercellular? *Plant Physiology* **86**: 200–203.

Nash JE, Sutcliffe JV. 1970. River flow forecasting through conceptual models part I – a discussion of principles. *Journal of Hydrology* **10**: 282–290.

Nepstad DC, De Carvalho CR, Davidson EA, Jipp PH, Lefebvre PA, Negreiros GH, Da Silva ED, Stone TA, Trumbore SE, Vieira S. 1994. The role of deep roots in the hydrological and carbon cycles of Amazonian forests and pastures. *Nature* **372**: 666–669.

Ocheltree TW, Nippert JB, Prasad PVV. 2016. A safety vs efficiency trade-off identified in the hydraulic pathway of grass leaves is decoupled from photosynthesis, stomatal conductance and precipitation. *New Phytologist* **210**: 97–107.

Powell TL, Galbraith DR, Christoffersen BO, Harper A, Imbuzeiro HMA, Rowland L, Almeida S, Brando PM, da Costa ACL, Costa MH *et al.* 2013. Confronting model predictions of carbon fluxes with measurements of Amazon forests subjected to experimental drought. *New Phytologist* **200**: 350–365.

Prentice IC, Dong N, Gleason SM, Maire V, Wright IJ. 2014. Balancing the costs of carbon gain and water transport: testing a new theoretical framework for plant functional ecology. *Ecology letters* **17**: 82–91.

Qu X, Cao B, Kang J, Wang X, Han X, Jiang W, Shi X, Zhang L, Cui L, Hu Z *et al.* 2019. Fine-tuning stomatal movement through small signaling peptides. *Frontiers in Plant Science* **10**: 69.

Restrepo-Coupe N, Levine NM, Christoffersen BO, Albert LP, Wu J, Costa MH, Galbraith D, Imbuzeiro H, Martins G, da Araujo AC *et al.* 2017. Do dynamic global vegetation models capture the seasonality of carbon fluxes in the Amazon basin? A data-model intercomparison. *Global Change Biology* **23**: 191–208.

Rogers A, Medlyn BE, Dukes JS, Bonan G, von Caemmerer S, Dietze MC, Kattge J, Leakey ADB, Mercado LM, Niinemets U *et al.* 2017. A roadmap for improving the representation of photosynthesis in Earth system models. *New Phytologist* **213**: 22–42.

Rowland L, Da Costa ACL, Galbraith DR, Oliveira RS, Binks OJ, Oliveira AAR, Pullen AM, Doughty CE, Metcalfe DB, Vasconcelos SS *et al.* 2015. Death from drought in tropical forests is triggered by hydraulics not carbon starvation. *Nature* **528**: 119–122.

Saleska SR, da Rocha HR, Huete AR, Nobre AD, Artaxo P, Shimabukuro YE. 2013. *LBA-ECO CD-32 flux tower network data compilation, Brazilian Amazon: 1999–2006. Data set.* Oak Ridge, TN, USA: Oak Ridge National Laboratory Distributed Active Archive Center.

Savage VM, Bentley LP, Enquist BJ, Sperry JS, Smith DD, Reich PB, von Allmen EI. 2010. Hydraulic trade-offs and space filling enable better predictions of vascular structure and function in plants. *Proceedings of the National Academy of Sciences, USA* **107**: 22722–22727.

Sellers PJ. 1985. Canopy reflectance, photosynthesis and transpiration. *International Journal of Remote Sensing* **6**: 1335–1372.

Sheffield J, Wood EF. 2008. Projected changes in drought occurrence under future global warming from multi-model, multi-scenario, IPCC AR4 simulations. *Climate Dynamics* **31**: 79–105.

Sitch S, Huntingford C, Gedney N, Levy PE, Lomas M, Piao SL, Betts R, Ciais P, Cox P, Friedlingstein P *et al.* 2008. Evaluation of the terrestrial carbon cycle, future plant geography and climate-carbon cycle feedbacks using five Dynamic Global Vegetation Models (DGVMs). *Global Change Biology* **14**: 2015–2039.

Sperry JS. 2004. Coordinating stomatal and xylem functioning–an evolutionary perspective. *New Phytologist* **162**: 568–570.

Sperry JS, Venturas MD, Anderegg WRL, Mencuccini M, Mackay DS, Wang Y, Love DM. 2017. Predicting stomatal responses to the environment from the optimization of photosynthetic gain and hydraulic cost. *Plant Cell and Environment* **40**: 816–830.

Stocker BD, Zscheischler J, Keenan TF, Prentice IC, Peñuelas J, Seneviratne SI. 2018. Quantifying soil moisture impacts on light use efficiency across biomes. *New Phytologist* **218**: 1430–1449.

Trugman AT, Medvigy D, Mankin JS, Anderegg WRL. 2018. Soil moisture stress as a major driver of carbon cycle uncertainty. *Geophysical Research Letters* **45**: 6495–6503.

Ukkola AM, De Kauwe MG, Pitman AJ, Best MJ, Abramowitz G, Haverd V, Decker M, Haughton N. 2016. Land surface models systematically overestimate the intensity, duration and magnitude of seasonal-scale evaporative droughts. *Environmental Research Letters* **11**: 104012.

Venturas MD, Sperry JS, Love DM, Frehner EH, Allred MG, Wang Y, Anderegg WRL. 2018. A stomatal control model based on optimization of

carbon gain versus hydraulic risk predicts aspen sapling responses to drought. *New Phytologist* **220**: 835–850.

Walsh RPD, Lawler DM. 1981. Rainfall seasonality: description, spatial patterns and change through time. *Weather* **36**: 201–208.

Wang Y, Sperry JS, Venturas MD, Trugman AT, Love DM, Anderegg WR. 2019. The stomatal response to rising CO_2 concentration and drought is predicted by a hydraulic trait-based optimization model. *Tree Physiology* **39**: 1416–1427.

Williams M, Rastetter EB, Fernandes DN, Goulden ML, Wofsy SC, Shaver GR, Melillo JM, Munger JW, Fan SM, Nadelhoffer KJ. 1996. Modelling the soil-plant-atmosphere continuum in a Quercus-acer stand at Harvard forest: the regulation of stomatal conductance by light, nitrogen and soil/plant hydraulic properties. *Plant, Cell & Environment* **19**: 911–927.

Winkler AJ, Myneni RB, Alexandrov GA, Brovkin V. 2019. Earth system models underestimate carbon fixation by plants in the high latitudes. *Nature Communications* **10**: 885.

Wolf A, Anderegg WRL, Pacala SW. 2016. Optimal stomatal behavior with competition for water and risk of hydraulic impairment. *Proceedings of the National Academy of Sciences, USA* **113**: E7222–E7230.

Wolfe BT, Sperry JS, Kursar TA. 2016. Does leaf shedding protect stems from cavitation during seasonal droughts? A test of the hydraulic fuse hypothesis. *New Phytologist* **212**: 1007–1018.

Worrall JJ, Marchetti SB, Egeland L, Mask RA, Eager T, Howell B. 2010. Effects and etiology of sudden aspen decline in southwestern Colorado, USA. *Forest Ecology and Management* **260**: 638–648.

Xu X, Medvigy D, Powers JS, Becknell JM, Guan K. 2016. Diversity in plant hydraulic traits explains seasonal and inter-annual variations of vegetation dynamics in seasonally dry tropical forests. *New Phytologist* **212**: 80–95.

Supporting Information

Additional Supporting Information may be found online in the Supporting Information section at the end of the article.

Fig. S1 Responses of Eqns 4 and 5 to environmental drivers.

Fig. S2 Maps of the observation sites used on this study.

Fig. S3 Agreement between numerical and analytical SOX.

Fig. S4 Daily drought evolution modelled by JULES and JULES-SOX.

Fig. S5 Differences between evapotranspiration predicted by JULES and JULES-SOX.

Fig. S6 Seasonal variation in modelled and observed evapotranspiration.

Fig. S7 Seasonal variation in modelled and observed soil moisture.

Notes S1 Analytical SOX derivation.

Notes S2 Computing A and V numerical derivatives.

Notes S3 Leaf photosynthesis model solved for stomatal conductance.

Notes S4 Whole-tree hydraulic conductance and xylem tapering calculations.

Table S1 Details for the data used in the SOX leaf-level evaluation.

Table S2 Sites used for the ecosystem-level evaluation of JULES-SOX.